

Droplet generation in a microchannel with a controllable deformable wall

A. Raj¹ · R. Halder¹ · P. Sajeesh¹ · A. K. Sen¹ 

Received: 17 January 2016 / Accepted: 21 June 2016 / Published online: 29 June 2016
© Springer-Verlag Berlin Heidelberg 2016

Abstract We report the droplet generation behavior of a microfluidic droplet generator with a controllable deformable membrane wall using experiments and analytical model. The confinement at the droplet generation junction is controlled by using external pressure, which acts on the membrane, to generate droplets smaller than junction size (with other parameters fixed) and stable and monodispersed droplets even at higher capillary numbers. A non-dimensional parameter, i.e., controlling parameter K_p , is used to represent the membrane deformation characteristics due to the external pressure. We investigate the effect of the controlled membrane deformation (in terms of K_p), viscosity ratio λ and flow rate ratio r on the droplet size and mobility. A correlation is developed to predict droplet size in the controllable deformable microchannel in terms of the controlling parameter K_p , viscosity ratio λ and flow rate ratio r . Due to the deflection of the membrane wall, we demonstrate that the transition from the stable dripping regime to the unstable jetting regime is delayed to a higher capillary number Ca (as compared to rigid droplet generators), thus pushing the high throughput limit. The droplet generator also enables generation of droplets of sizes smaller than the junction size by adjusting the controlling parameter.

1 Introduction

Droplets suspended in an immiscible fluid have numerous applications including encapsulation of target cells (Chabert

and Viovy 2008; Kemna et al. 2012), drug delivery (Vladislavljjevic et al. 2013), tumor destruction (Yoshida et al. 2005), printing technology (Sen and Darabi 2007), chemical analysis and precise mixing of reagents (Sarrazin et al. 2007) and as ultrasound agents (Reznik et al. 2011). The uniformity in the size distribution of droplets is an important criterion to determine the quality of emulsion (Link et al. 2006). Droplet emulsions have unique flow characteristics including the variation of viscosity with shear rate and increased elasticity due to the surface tension provided by droplets. Initially, microdroplets were produced in bulk media using conventional methods including spray drying (Vehring et al. 2007), membrane emulsification (Charcosset et al. 2004), agitation (Lignel et al. 2014), large-scale blenders (Huebner et al. 2008) and high speed mixing (Sugiura et al. 2001). Although the coefficient of variation in the size of droplets can be reduced by using a homogenizer with high frequency, microdroplets produced by the above methods have large polydispersity. Later, microfluidic devices, which use external electric fields (Link et al. 2006), microinjectors and needles (Yang et al. 2010; Meesters et al. 1992) were used for the emulsification process. However, simple microfluidic devices, which produce microdroplets with low polydispersity (Christopher and Anna 2007; Sajeesh et al. 2014; Surya et al. 2014), by exploiting the flow instabilities of two laminar immiscible fluids, paid significant attention. High-throughput droplet generation and ability to carry out biological and chemical reactions in nanolitre-sized droplets make the emulsification process in microfluidic devices very attractive. Different configurations of microchannel including T-junction (Christopher and Anna 2007; Gupta and Kumar 2010), double T-junction (Surya et al. 2014), flow focusing (Adzima and Velankar 2006; Sajeesh et al. 2014) and co-flowing (Umbanhowar et al. 2000) were widely used for the emulsification process.

✉ A. K. Sen
ashis@iitm.ac.in

¹ Department of Mechanical Engineering, Indian Institute of Technology Madras, Chennai 600036, India

Droplet breakup in a microfluidic device can be classified into different regimes viz., squeezing, dripping and jetting. Monodisperse droplets with uniform interdistance between them are preferred in most emulsification processes, which can be achieved with the droplet breakup in squeezing and dripping regimes. In the jetting regime, the droplet production is highly unstable and the spacing between the droplets is not uniform. Additionally, the formation of secondary droplets makes the emulsion polydispersed. Breakup mechanism can be further stabilized by decreasing the width of the discrete phase to half the width of the main channel (Garstecki et al. 2006). This reduces the formation of the secondary droplets during droplet breakup (van der Graaf et al. 2006). Also, it has been widely reported that the minimum size of the droplets formed in a microchannel is limited by the dimensions of the droplet breakup junction (Garstecki et al. 2006; Sajeesh et al. 2014; Surya et al. 2014). The influence of flow rate ratio r (ratio of the flow rates of the discrete phase to that of the continuous phase), viscosity ratio λ (ratio of the viscosity of the discrete phase to that of the continuous phase) and the capillary number (Ca) (i.e., interplay between surface tension and viscous forces and defined as $Ca = \mu U/\sigma$, where U is the velocity of the continuous phase flow, μ is the dynamic viscosity of the continuous phase fluid, and σ is the interfacial tension of the discrete and continuous phase interface) on the size of the droplets formed at a T-junction is well studied in the literature, and correlations are reported (Adzima and Velankar 2006; Christopher and Anna 2007; Gupta and Kumar 2009). However, in a flow-focusing device, one single model cannot be used to correlate the droplet breakup as a function of various control parameters (Christopher and Anna 2007; Nie et al. 2008). It is reported that, at low Ca and viscosity ratio, the size of the droplet formed is governed by the flow rate ratio of the two phases (Zhang and Stone 1997). Also, numerical simulations show a weak dependence of viscosity ratio on the droplet breakup even at low Ca (Garstecki et al. 2005). It is reported that the size of droplets can be reduced by increasing the viscosity ratio of droplets, but at high viscosity ratios, the monodispersity of the droplets can be achieved only at low flow rates, which reduces throughput (Sajeesh et al. 2014).

Recently, it is reported that the formation of droplets in a soft microchannel reduces the polydispersity of droplets (Pang et al. 2014). In another work, the droplet breakup junction included a controllable moving-wall structure, which enabled the formation of droplets of size smaller than the junction diameter (Lin et al. 2008). External pressure was used to actuate the moving-wall structure for tuning the droplet size. Similarly, a flow-focusing microfluidic droplet generator with a controllable moving-wall chopper was used to control the diameter of the droplets formed

(Hsiung et al. 2006; Lee et al. 2007). Although the above works extensively deal with the control of the droplet size, the effect of the deformability of the flexible wall and the wall deformation on the droplet formation is not studied. Further, the physical understanding of droplet formation, including the flow regimes, in a deformable microchannel is limited. Classical correlations reported in the literature are not suitable for predicting the droplet diameter in a deformable droplet generation device. In a deformable droplet generator, in addition to the fluid and flow parameters, a parameter that represents the effect of the deformation of the deformable wall also needs to be considered.

In the literature, many works have been reported on the formation of smaller monodisperse droplets with uniform interdistance in a microchannel, as discussed above. It is found that the reaction rate of chemicals in droplet microreactors increases with decrease in the size of droplets. However, the size of droplets is often limited by the junction size of the droplet generators since the fabrication of droplet generators with smaller junction size is challenging. In the present work, we report use of a microfluidic droplet generator which enables generation of droplets of size smaller than the junction size by using deformable microchannel walls. The confinement at the droplet generation junction is controlled using external pressure acting on the deformable wall. It is possible to adjust the external pressure and control the deformation of the deformable wall to generate droplets of size varying over a range, at a fixed flow rate ratio, which is not possible using a rigid droplet generator. The size range of droplets formed in a rigid droplet generator can be increased by changing the depth of the droplet junction. However, in such rigid droplet generators, since the droplet size is limited by the depth at the junction, in order to achieve a wider range of droplet size, devices with different junction heights need to be fabricated, which is time consuming and expensive. But, by using the proposed controlled deformable droplet generator, height of the device at the droplet junction can be dynamically controlled by changing the external pressure to generate droplets of a wider size range. A non-dimensional parameter, i.e., controlling parameter K_p , is used to represent the characteristics of membrane deformation due to the external pressure. We investigate the effect of the controlled membrane deformation (in terms of K_p), viscosity ratio λ and flow rate ratio r on the droplet size and mobility. A correlation is developed to predict droplet size in a controllable deformable microchannel in terms of the controlling parameter, viscosity ratio and flow rate ratio for a deformable droplet generator. We demonstrate that in a deformable droplet generator, due to the deflection of the wall, the transition from the stable dripping regime to the unstable jetting regime is delayed to a higher capillary number Ca , thus pushing the high throughput limit

(as demonstrated experimentally). Also, we demonstrate that the droplets generated using the proposed droplet generator with deformable walls are monodisperse (i.e., less polydispersed as compared to an similar size rigid droplet generator). The proposed device can very well be used for the applications where a dynamic change in droplet size is required such as cell encapsulation, drug delivery and diagnostics apart from other conventional microdroplet applications. To encapsulate and contain single or small number of biological cells, microdroplets can be an ideal vessel (Kohler and Henkel 2005). Since biological cell lines have wide range of sizes, we must need monodisperse microdroplets of different sizes produced dynamically in a single device so as to encapsulate cells of varying sizes and fetch it to the sensing area in order to probe their metabolites. Also in the case of drug delivery, precise amount of drug must be aimed, which can very well be achieved using the proposed device. Further, in order to perform controlled clinical laboratory tests, reagents of fixed amounts in the

form of monodispersed microdroplets can be incorporated for diagnostic applications using the proposed device. First, a brief description of the controllable deformable droplet generator is provided. Next, a theoretical model is presented for predicting the deflection of the deformable membrane and finding out the effective junction size at the droplet generation junction. Then, the device fabrication protocol, experimental setup and materials and methods are detailed. Finally, important results are presented and discussed.

2 Device description

A schematic of the proposed deformable droplet generator device is shown in Fig. 1. The device has two microchannels viz. droplet channel and controlling channel, with a thin PDMS membrane sandwiched between the two microchannels. The droplet channel contains a droplet generator

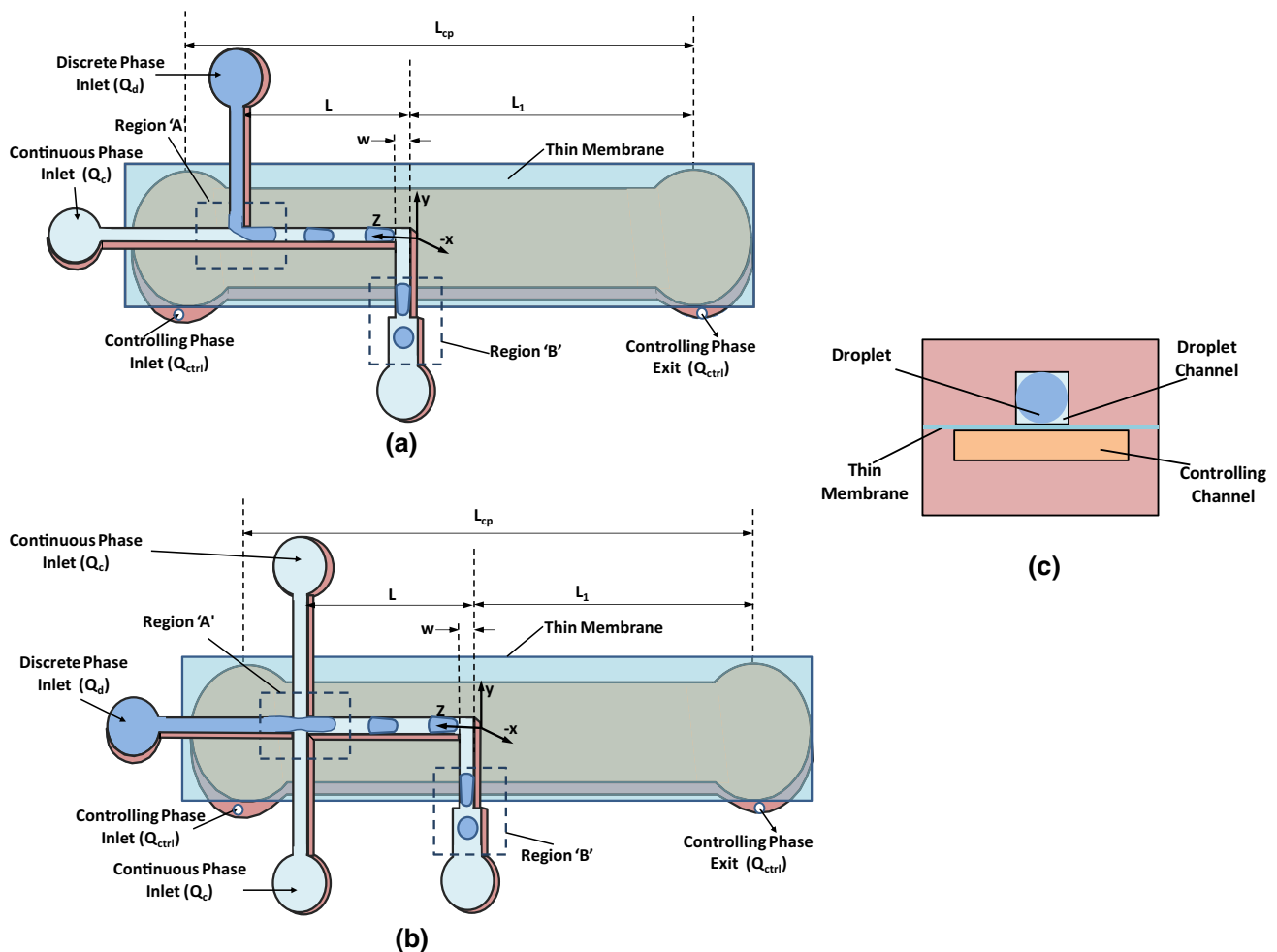


Fig. 1 Schematic of the controllable deformable T-junction droplet generator device. **a** Top view of T-junction deformable droplet generator. **b** Top view of flow-focusing deformable droplet generator. **c** Cross-sectional view of junction region

section for generating aqueous glycerol droplets (discrete phase) in mineral oil (continuous phase). Instead of compressed air, which is normally used for applying external pressure, in this case, a high-viscosity fluid (silicone oil) is pumped into the controlling channel to apply an external pressure on the membrane. Thus, it was possible to create a gradient of the pressure acting on the membrane, with the pressure taking a maximum value only at the droplet generator junction, where it is required. The flow rate through the controlling channel is adjusted to control the external pressure and thus the height of the droplet channel at the droplet generator junction, which affects the droplet formation. In addition to the external pressure acting on the membrane, the width of the membrane and the flexural rigidity of the membrane also affect the membrane deflection, whose combined effect is represented in terms of a non-dimensional parameter (i.e., controlling parameter K_p). The device is divided into two distinct regions: the 'region A' represents the droplet generation region, which is influenced by the external pressure due to the controlling channel, and 'region B', which is outside the purview of the external pressure. In 'region B', the width of the micro-channel is increased to measure the undeformed diameter of the droplets. When the pressure inside the controlling channel acting on the membrane exceeds the pressure inside droplet channel, the membrane deflects inward into the droplet channel and thus changes the effective height of the junction which in turn affect the droplet generation. Conventional rigid PDMS microfluidic droplet generators are used for comparing the performances with that of the deformable droplet generators.

We have used T-junction droplet generators for all of our experiments except for the generation of droplets less than junction diameter and capillary number dependence of droplet generation in which flow-focusing design was used. The choices of the T-junction and flow-focusing junction for different result sections are as follows. T-Junction devices are reported for investigating the

variation in droplet size by varying different parameters including the flow rate ratio r , viscosity ratio λ and controlling parameter K_p for fixed Ca number and develop a correlation for the size of the droplet produced in terms of these parameters. It is reported in the literature that simple scaling laws to predict the droplet size are not possible in terms of governing parameters, since droplet breakup in flow-focusing device is characterized by the large number of geometrical aspect ratios (Baroud et al. 2010). So in order to formulate a correlation for the size of the droplets formed in a deformable microchannel in terms of the governing parameters, we have used the T-Junction. It was evident from our experiments that, for the same governing parameters, flow-focusing device can produce smaller and uniform droplets as compared to T-junction. However, the smallest diameter of the droplets formed in a flow-focusing junction is limited by the size of the junction used. Thus, in order to demonstrate formation of smaller and uniform droplets over larger size range, we have performed our experiments using the flow-focusing junction and studied the effect of Ca number on the flow regimes using deformable flow-focusing device.

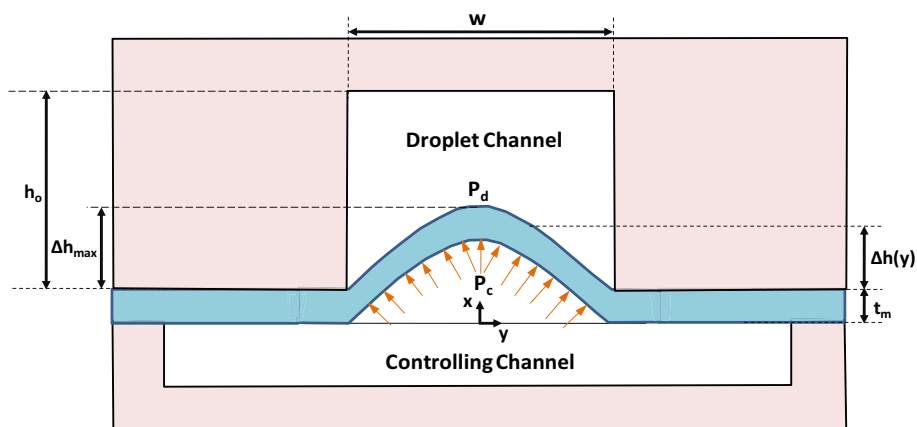
3 Theoretical model

A schematic of deformed channel cross section due to the external pressure acting on the deformable membrane is depicted in Fig. 2. In order to find out the variation in the channel height along the z -direction $h(z)$, the effective channel deflection Δh is estimated using the width-averaged displacement $\langle \Delta h \rangle$ as follows,

$$\frac{\Delta A}{A_0} = \frac{w \langle \Delta h \rangle}{wh_0} = \frac{\langle \Delta h \rangle}{h_0} \quad (1)$$

where A_0 and h_0 are the area of cross section and height of the droplet channel, when the membrane is in its

Fig. 2 Cross-sectional image of the double-layered device at the junction of the droplet generator section, pressure in the controlling channel is higher than that in the droplet channel



undeformed state, ΔA is the change in the area of cross section due to membrane deflection, w is the width of the droplet channel. At a particular location z along the channel, the effective channel height is expressed as

$$h(z) = h_0 \left(1 - \frac{\langle \Delta h \rangle (z)}{h_0} \right) \tag{2}$$

Assuming small deflection, at a particular cross section, the deflection profile is assumed to be parabolic as follows,

$$\Delta h(y) = \Delta h_{\max} \left(1 - 4 \frac{y^2}{w^2} \right) \tag{3}$$

where Δh_{\max} is the maximum deflection of the membrane at a particular location z , which occurs at $y = 0$. Thus, the relationship between the maximum and the average displacement is obtained as $\langle \Delta h \rangle \sim \frac{2}{3} \Delta h_{\max}$. So, we obtain the effective channel height as follows,

$$h(z) = h_0 \left(1 - \frac{2}{3} \frac{\Delta h_{\max}(z)}{h_0} \right) \tag{4}$$

The expression for Δh_{\max} in terms of the local pressure $p(z) = p_c(z) - p_d(z)$ can be found by performing a force balance on an infinitesimally small strip of the membrane wall as reported earlier (Raj and Sen 2016) and in appendix, as follows,

$$\Delta h_{\max}(z) = \left(\frac{3 w_d^4 (1 - \nu_m) [p_c(z) - p_d(z)]}{64 t_m E_m} \right)^{\frac{1}{3}} \tag{5}$$

where w_d is the width of the droplet channel, t_m is the membrane thickness, ν_m is the Poisson’s ratio and E_m is the Young’s modulus of the membrane material, $p_d(z)$ and $p_c(z)$ are the pressures values in the droplet and controlling channels, respectively. In the controlling microchannel, the pressure variation $p_c(z)$ is given by Bruus (2007). Since width of the controlling channel is around ten times higher than the width of the droplet phase channel, the deflection of the membrane will not have much effect on the cross-sectional area and hence fluid flow in the controlling channel. Hence, the pressure-flow characteristics for the controlling phase channel can be approximated similar to that of a rigid channel as

$$P_c(z) = \frac{12 \mu_c Q_c (z + L_1)}{w_c h_c^3 \left(1 - 0.63 \frac{h_c}{w_c} \right)} \tag{6}$$

where L_1 is the length between the ends of droplet and controlling channels (ref. Fig. 1), h_c and w_c are the height and width of the controlling phase channel, respectively. On the other hand, in the droplet channel, the effect of the

membrane deflection on the pressure-flow characteristics cannot be neglected since the width and the height of the channel are comparable to each other. The pressure along the droplet channel can be found by solving

$$-\frac{\partial p_d(z)}{\partial z} = \frac{12 \mu_{\text{eff}} Q_d}{w h^3 \left(1 - 0.63 \frac{h}{w} \right)} \tag{7}$$

where Q_d is the total flow rate in the droplet channel, $h = h(z)$ is the height of the droplet channel, which is given by Eq. 4, μ_{eff} is the effective viscosity of the two-phase flow (i.e., continuous phase and the droplet phase flowing through the droplet channel). Eqs. (4) and (7) are coupled in terms of $p_d(z)$, which are solved using MATLAB to obtain $p_d(z)$. Once we know $p_d(z)$, the maximum membrane deflection can be obtained using Eq. 5, which can be used further to determine the average deflection of the membrane as $\langle \Delta h \rangle = 2/3(\Delta h_{\max})$. Here, we represent the average wall deflection at the droplet generator junction as Δh_{th} and can be given as,

$$\Delta h_{\text{th}} = \langle \Delta h(z = L) \rangle = \frac{2}{3} \Delta h_{\max}(z = L) \tag{8}$$

To find out the effective viscosity μ_{eff} of the two-phase fluid (i.e., viscosity of the emulsion) in the droplet channel, we have taken a similar approach reported by Sajeesh et al. (2014). The monodispersed droplets formed using a T-junction at the upstream of the device having uniform interdistance between them are allowed to flow through a test section of known length in a rigid (glass bonded) droplet microchannel. The differential pressure Δp_r across the test section is measured using a differential pressure sensor, which is used to predict the effective viscosity μ_{eff} as follows (Bruus 2007),

$$\mu_{\text{eff}} = \frac{\Delta p_r w h_r^3 \left(1 - \frac{192}{\pi^5} \frac{h_r}{w} \sum_{n=\text{odd}}^{\infty} \frac{1}{n^5} \tanh \left(n \pi w / 2 h_r \right) \right)}{12 Q_r L_t} \tag{9}$$

where h_r is the height and w is the width of the rigid microchannel used for the pressure drop measurements, L_t is the length of the test section in the rigid microchannel, and Q_r is the total flow rate.

From the literature, it is known that the Young’s modulus of thin PDMS membrane is a function of the membrane thickness and the processing parameters (Liu et al. 2009; Johnston et al. 2014) and varies considerably with thickness at low thickness range of membranes. So, in order to determine the Young’s modulus of the membrane, we have used the analytical model reported earlier (Raj and Sen 2016) for the deflection profile of a deformable microchannel, which is given as follows

$$\begin{aligned} & \left(\frac{w}{4h_0}\right)h^4 - \left(\frac{2w + 0.63h_0}{5h_0^2}\right)h^5 + \left(\frac{w + 1.26h_0}{6h_0^3}\right)h^6 - \left(\frac{0.09}{h_0^3}\right)h^7 \\ & = \frac{1}{18} \frac{w^4 \mu (1 - \nu_m) Q}{t_m E_m h_0^3} (L - z) + \frac{1}{60} w h_0^3 - (0.006) h_0^4 \end{aligned} \quad (10)$$

In order to determine the Young's modulus of a thin membrane, it was bonded over a straight channel such that the thin membrane acts as one of the four walls of the straight microchannel. Please note that in this case, the other side of the thin membrane wall is open to atmosphere and there is no controlling channel used in this case. So the membrane wall deflects outward giving rise to an increased effective height of the microchannel. Hence, $\Delta h_{(\max)}(z)$ is negative in this case. We have performed fluorescence imaging to measure the deflection of the thin deformable wall $h(z)$ at a particular location z along the microchannel. Since all the other parameters including w , h_0 , μ , ν_m , t_m and L are known, the Young's modulus E_m of the thin PDMS membrane can be determined using Eq. 10.

4 Experiments

4.1 Device fabrication

We used photolithography followed by soft lithography (Sajeesh et al. 2014) to fabricate the double-layered PDMS microchannel. The two microchannel layers (droplet and controlling channels) were fabricated separately and then bonded together with a thin membrane sandwiched between them. For the fabrication of thin PDMS membranes, degassed mixture of PDMS was mixed with 20 % hexane so as to increase its flexibility (Thangawng et al. 2007). Then, the mixture was spun coated onto a clean PMMA sheet of $10 \times 5 \times 0.3$ cm size at 2500 rpm for 85 s at an acceleration of 8 rpm/s. The PDMS-coated PMMA sheet was then cured inside vacuum oven for 6 h. After the thin PDMS layer on the PMMA sheet was cured, it was bonded on top of the PDMS droplet channel using oxygen-plasma bonding such that it acts as one of the walls of the flow-focusing channel. Once the droplet generation device was fabricated, it was bonded with the controlling channel so that droplet and the controlling channels were aligned and thin PDMS membrane was sandwiched between the two channels. Finally, PTFE tubings (Cheminert fittings-VICI, Germany) were glued to the access holes to establish fluidic connection. The width of controlling phase channel and focussing channel fabricated was 1000 and 100 μm , respectively. Cross-sectional view of the bonded device was captured using an inverted microscope (Axiovert A, Carl Zeiss, Germany) attached with a high speed camera (Photron SA3, USA). The cross-sectional view showing the droplet and controlling channels and the thin membrane

sandwiched between the channels is shown in Fig. 3b. The thickness of thin PDMS layer fabricated was measured to be $22.5 \pm 2 \mu\text{m}$.

4.2 Materials and methods

Mineral oil (Fisher scientific-Across organics, New Jersey, USA) with 5 % wt/wt of Span 85 (Sigma Life sciences, USA), of viscosity 0.0287 Pa s (Sajeesh et al. 2014) was used as the continuous phase. For the viscosity ratio dependence study, mixtures of DI water and aqueous glycerol at different concentrations viz. 40 and 60 % (corresponding mixture of viscosities 0.003237, 0.0086 Pa s, respectively; Sajeesh et al. 2014) were used as discrete phase. Interfacial tension value of mineral oil (with 5 % wt/wt of Span 85) and aqueous solution interface can be found from our earlier work (Sajeesh et al. 2014). Rhodamine dye was mixed thoroughly with mineral oil at a concentration of 2 % by volume to get the illumination, and fluorescence imaging was used to determine the effective junction height of the droplet generator. Si-oil (Sigma-Aldrich, Germany) of viscosity 1.0 Pa s was infused through the controlling channel to apply the external pressure on the thin membrane. It is not necessary to use only oil to infuse through the controlling channel. In fact, any highly viscous liquid can be used because in that case a small change in flow rate of the controlling fluid can produce significant modification in pressure in the controlling channel. This modification in pressure causes the thin membrane to deflect inward toward the droplet generator channel, thus reducing the junction height of the droplet generator. Water can also be used as the controlling phase, but since the viscosity of water is low, in that case much higher flow rate is required to create the same pressure difference across the thin membrane. The viscosity of Si-oil (Sigma-Aldrich, Germany) is 1.0 Pa s, which is around 1000 times higher than that of water and therefore was selected as the controlling phase in our experiments.

4.3 Experimental setup

Syringe pumps (TSE systems, Germany and Lucca Technologies, Harwinton) were used for infusing the continuous phase, discrete phase and controlling phase liquids (refer Fig. 3a). For the pressure drop measurements, piezoresistive-type differential pressure sensor PX26–005DV with a DP25B S-230A display unit (Omega Stanford, USA) was used, which is capable of measuring transient pressure drop with response time of approximately 1.0 ms. The pressure sensor was interfaced with the microfluidic device with the help of connectors and PTFE tubing. In order to avoid the possibility of oil–air interface inside the capillary, the capillaries connecting the pressure taps on the device and the

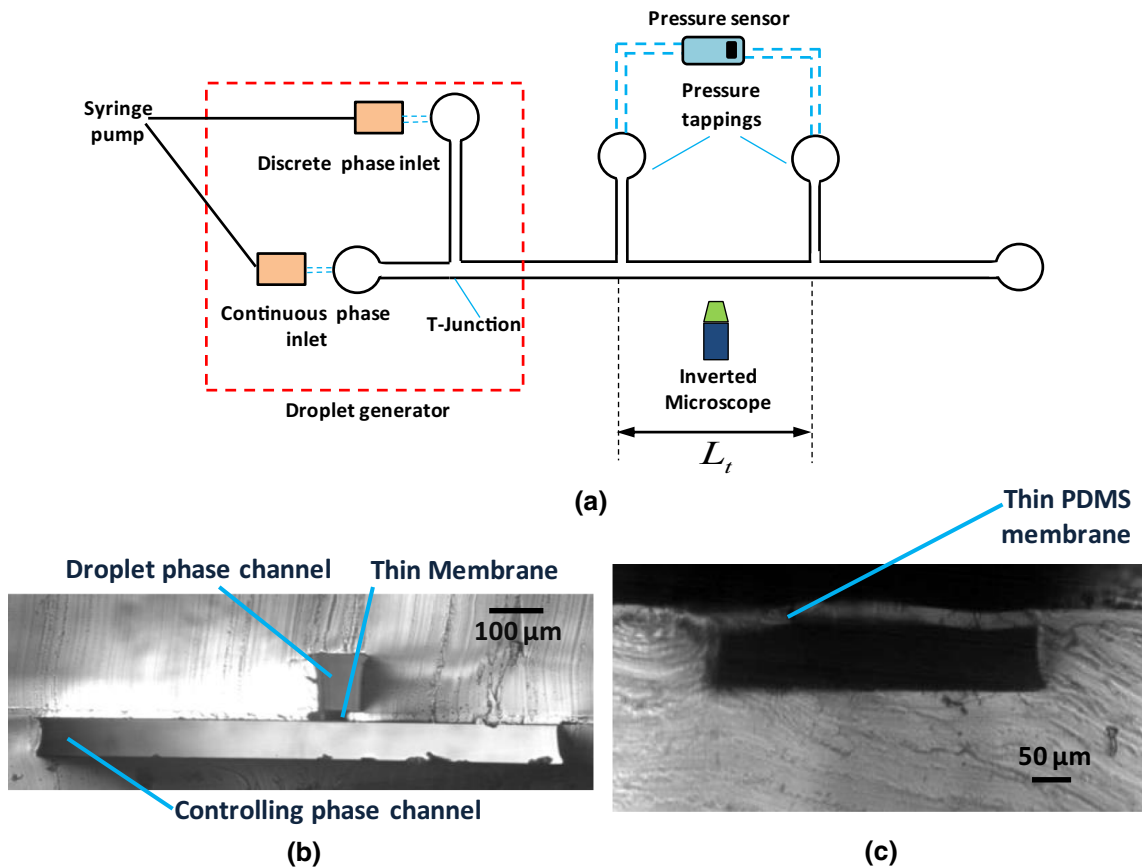


Fig. 3 **a** Schematic diagram of microfluidic chip used for effective viscosity measurement (Sajeesh et al. 2014). **b** Cross-sectional view of deformable droplet generator device. **c** Cross-sectional image of

channel used for Young’s modulus measurement, Young’s modulus of the thin membrane used as the *top wall* is determined

pressure sensor were primed carefully. We have used the similar protocol followed by Cheung et al. (2012) to interface the pressure sensor with the pressure tapplings and perform the experiments with the pressure sensor. An inverted microscope (Axiovert A1) coupled with a high speed camera (FASTCAM SA3, Photron Inc., USA) and fluorescent attachment (HBO 100 illuminator, Carl Zeiss, Germany) interfaced with PC via software (Photron Fastcam Viewer 3) was used to capture the images. Fluorescence imaging was used to measure the deflection of the thin membrane by analyzing the captured images using Image J software. The procedure used for measuring and calculating the deflection is reported in our earlier works (Anoop and Sen 2015; Raj and Sen 2016). The experiments were performed inside an air-conditioned laboratory at a temperature of 24 °C to eliminate the influence of temperature on the liquid properties. Pressure drop across the test section ($L_t = 10$ mm) in the microchannel was measured using a pressure sensor as shown in Fig. 3a. The cross-sectional optical image of the microfluidic deformable channel used for the Young’s modulus measurements is shown in Fig. 3c.

5 Results and discussion

5.1 Effective viscosity of droplet phase and Young’s modulus measurement

As explained in Sect. 3, the effective viscosity of the droplet phase and the Young’s modulus of membrane material are required to find out the maximum deflection of the deformable membrane wall. First, for the measurement of the effective viscosity of emulsion, pressure drop measurements were performed using an experimental setup schematically shown in Fig. 3a, at different flow rate ratios r . The measurements were performed at a capillary number $Ca = 0.03$ and viscosity ratio $\lambda = 0.03$. From the pressure drop values, the effective viscosity of the two-phase fluid in the microchannel was predicted using Eq. 9, which was later used for calculating the maximum membrane deflection. The variation of effective viscosity of the two-phase fluid with the flow rate ratios is presented in Fig. 4a. The effective viscosity is calculated from the pressure drop produced by the emulsion in the

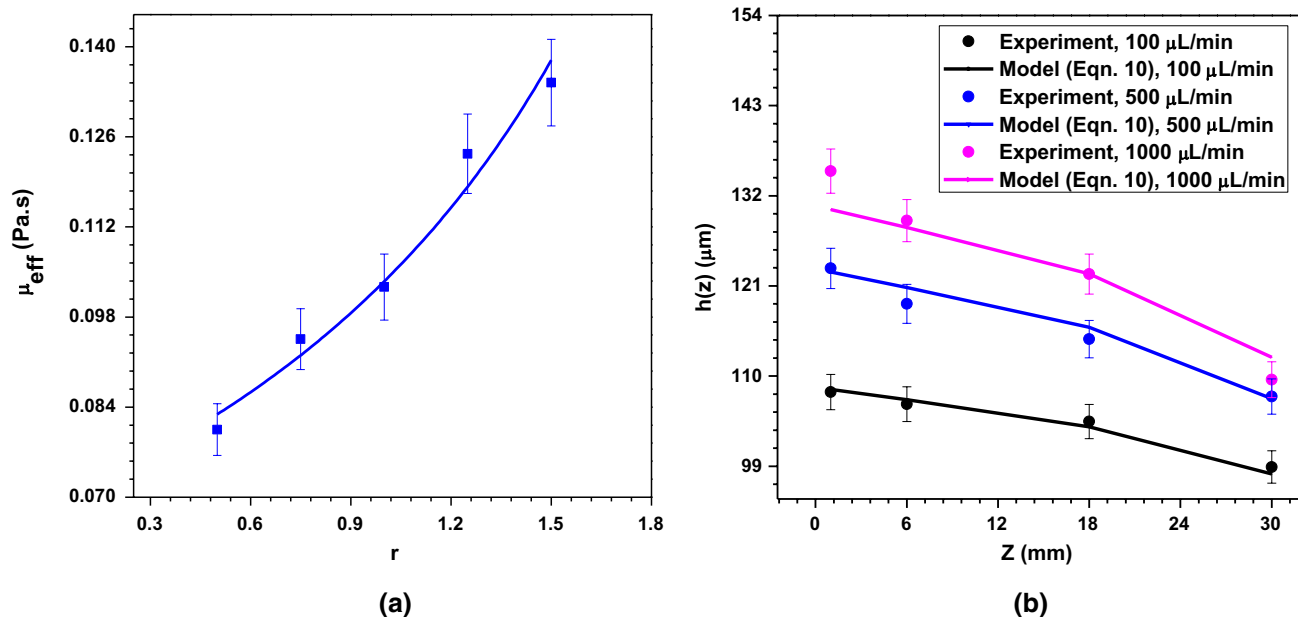


Fig. 4 **a** Effective viscosity versus flow rate ratio, $Ca = 0.03$ and $\lambda = 0.03$, *solid line* shows fitting of the experimental data. **b** Effective channel height of the straight microchannel with the thin membrane (whose Young's modulus is to be found out) as one of its wall along the length. One of the data point was used to reverse calculate the

test section. Additional pressure drop offered by the droplets is negligible for droplet size ratio (ratio of the droplet size to the channel size) less than 0.5 (Sajeesh et al. 2014). Thus theoretically, when the flow rate ratio r tends to zero, the size ratio of the droplets is negligible and the pressure drop produced across the test section would be same as that by the continuous phase alone. Thus, the effective viscosity would become equal to the continuous phase viscosity. However, at flow rate ratios $r \gg 1$, the size ratio of the droplets generated is greater than 0.5; thus, the additional pressure drop produced by the droplets increases. This increases the net pressure drop in the test section as mentioned above and hence the effective viscosity. Further, it is observed from Fig. 4a that, as the flow rate ratio r increases, the effective viscosity μ_{eff} increases nonlinearly with the increase in the flow rate ratio r .

Further, Young's modulus of the membrane material was found out from the membrane deflection, which is measured using the fluorescence intensity across the channel cross section. A straight microchannel of dimensions $w = 500 \mu\text{m}$, $h_0 = 83 \mu\text{m}$ and $L = 36 \text{mm}$ with the thin membrane bonded as one of its wall was used for the experiment. The maximum membrane deflection Δh_{max} ($z = 18 \text{mm}$) for a flow rate of $Q = 1000 \mu\text{L}/\text{min}$ was measured to be $59.2 \mu\text{m}$, which gives the effective channel height of the thin membrane wall as $h = 122.5 \mu\text{m}$. By using these parameters in

value of the young's modulus using Eq. 10, which when used for the other data points to predict the effective channel height, show a good agreement with the experimental result with a maximum error of 5%. The *solid line* here represents the model (Eq. 10), and the points are the experimental data

Eq. 10, the Young's modulus of the membrane E_m was calculated as 1.842 MPa. Next, we used Eq. 9 to predict the variation of the effective channel height $h(z) = h_0 + \langle \Delta h \rangle(z)$ along the length of the channel, for two different flow rates $Q = 100$ and $1000 \mu\text{L}/\text{min}$, as shown in Fig. 4b. The effective channel height was measured using fluorescence imaging experiments at four different locations along the channel length, for two different flow rates, as shown in Fig. 4b. The model predictions compare well with the experimental results within a maximum error of 5%. A very good match between the experimental data and model predictions confirms the predicted value of Young's modulus of the membrane (at two different flow rate ratios).

5.2 Controlling parameter and membrane deflection at junction

We introduce a non-dimensional controlling parameter K_p to represent the effect of membrane actuation on droplet size, which is defined as follows,

$$K_p = \frac{w_t^3 \Delta p_t}{D} \quad (11)$$

where w_t is the width of the droplet channel at the junction, Δp_t is the pressure difference acting on the membrane at the junction (i.e., difference between the controlling and droplet channel pressure across the membrane at the

junction) and D is the flexural rigidity of the thin membrane wall material which is given by the following expression,

$$D = \frac{E_m t_m^3}{(1 - \nu^2)} \tag{12}$$

where E_m is the Young’s modulus of the thin membrane material, t_m is the thickness of the thin membrane which is sandwiched between two channel (refer to Fig. 2), and ν is the Poisson’s ratio of the thin membrane material. Once we determine the value of the Young’s modulus of the membrane wall and measure the wall thickness, we can use the above expression for finding out the value of the flexural rigidity of the thin membrane wall. For flow rate ratio $r = 0.50$, viscosity ratio $\lambda = 0.03$ and capillary number $Ca = 0.03$, the deflection of the membrane at the junction was measured from experiments (using fluorescence imaging) and predicted using the model. The effect of the controlling parameter K_p on the membrane deflection at the junction is presented in Fig. 5. As observed, the deflection of the membrane predicted using the theoretical model matches well with that obtained from the experimental measurements (within 20 %). The difference between the model and the experimental results is mainly because of the low aspect ratio approximation used in Eq. 7. It is to be noted that, as compared to the complicated Fourier series expression of the flow rate profile in rectangular channel, Eq. 7 is accurate within 13 % for a limiting aspect ratio $\frac{h}{w} \sim 1$ (Bruus 2007). In addition, the pressure drop measurement involves variation in the pressure sensor output over a range (± 5 –10 %) giving rise to the total error of 5–20 %. When the pressure in the

controlling channel is equal to that in the droplet channel at the junction or the channel width is very small or flexural rigidity of the membrane wall is very high, then the controlling parameter $K_p = 0$. We observed that when the controlling parameter is zero, the membrane deflection is zero and in that case the droplet channel behaves as a rigid channel. When the pressure in the controlling channel at the junction is less than that in the droplet channel, the differential pressure across the membrane is negative (also controlling parameter K_p is negative) and thus the membrane deflects into the controlling channel and the channel deflection is found to be negative. When the controlling parameter is positive and increases due to increase in the differential pressure or increase in the channel width or decrease in membrane thickness of Young’s modulus, the membrane deflects more into the droplet channel and thus deflection of the membrane at the junction also increases, as shown Fig. 5. Once the pressure in the controlling channel is changed, the transition time of the droplet generation depends on the response time of the thin membrane wall. Due to the change in pressure, the membrane attains a modified deformed shape, thus giving rise to a new equivalent height of the junction which controls droplet size. The response time of a thin membrane to an applied load is given as $\tau = \sqrt{(\rho_s t_m l^4) / B}$, where ρ_s is membrane density, t_m is membrane thickness, l is the length and B is the bending stiffness per unit width of the thin membrane (Landau and Lifshitz 1986). It is clear that the response time reduces with decrease in the membrane thickness so the new equilibrium droplet size is obtained faster. In our experiments, it was observed that the system shifts from one equilibrium droplet size to another within 2 min (the syringe pumps used in our experiments also have some response time to react to the change in flow rate).

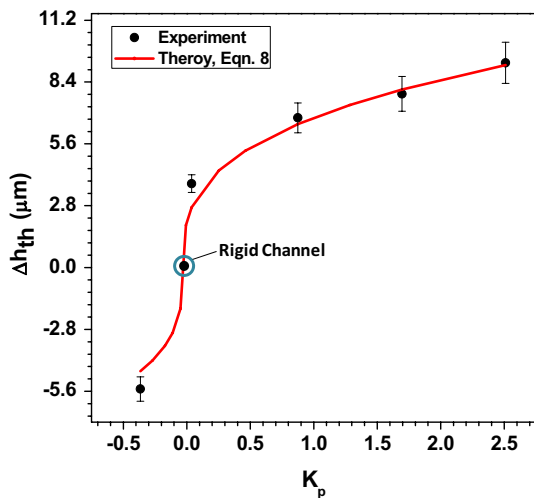
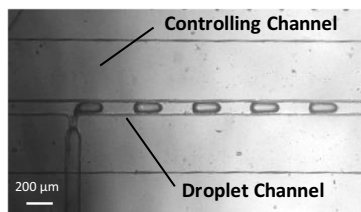


Fig. 5 Comparison of experiment and theory for the variation of change in junction height with controlling parameter K_p at flow rate ratio $r = 0.5$, viscosity ratio $\lambda = 0.03$ and capillary number $Ca = 0.03$

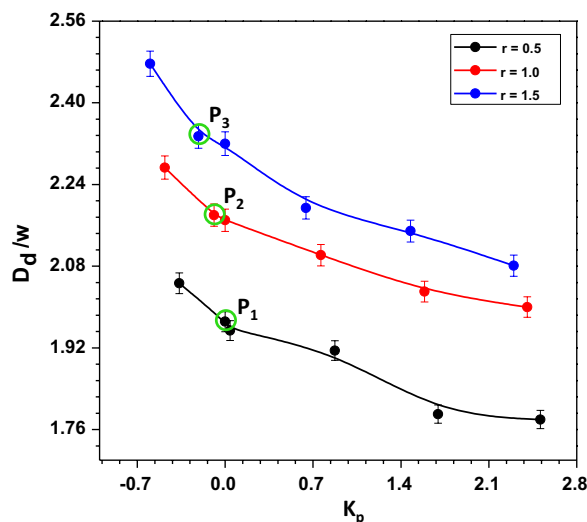
5.3 Effect of controlling parameter on droplet size

The top view of the droplet formation in the T-junction device is shown in Fig. 6a. As explained in Sect. 3, the width of the droplet generation channel is much smaller as compared to the width of the controlling phase channel. Experiments were carried out to study the effect of the controlling parameter K_p on droplet size, for different viscosity and flow rate ratios, while operating in the dripping regime (i.e., $Ca \leq 0.32$). In order to vary the controlling parameter K_p , we have varied the pressure in the controlling channel which essentially changes the pressure jump across the thin membrane at the junction Δp_r . In this regime, the viscous shear force offered by the continuous phase and the interfacial force are responsible for the droplet breakup. Figure 6b presents the non-dimensional droplet size variation with the controlling parameter, at different flow rate ratios and a fixed viscosity ratio $\lambda = 0.03$. The error bars

Fig. 6 **a** Image of droplet breakup using deformable T-junction droplet generator at controlling parameter $K_p = -0.3646$, flow rate ratio $r = 0.5$, viscosity ratio $\lambda = 0.03$ and $Ca = 0.032$. **b** Variation of non-dimensional droplet size with the controlling parameter K_p at various flow rate ratios r for viscosity ratio $\lambda = 0.03$ and $Ca = 0.032$. The green circled points correspond to controlling phase flow rate of $Q_{ctrl} = 1 \mu\text{L}/\text{min}$; solid line shows fitting of the experimental data (color figure online)



(a)



(b)

in the plots represent the standard deviation of the experimental data. In each device, at a particular flow rate ratio and viscosity ratio, the sizes of >50 droplets were measured and the experiments were repeated on at least three devices. At a fixed flow rate ratio, the droplet size decreases with the increase in the controlling parameter and at a fixed controlling parameter; the droplet size increases with the increase in flow rate ratios. When the controlling parameter K_p is zero, the diameter of the droplet generated in that case is same as that generated using an equivalent rigid microchannel. If the controlling parameter is negative, the diameter of the droplets is larger than that in case of a rigid channel (of size same as the undeflected channel size). When the controlling parameter is positive, diameter of the droplet formed will be smaller compared to the rigid channel at the same governing parameters. As the controlling parameter increases, the membrane deflection at the junction also increases (shown in Fig. 5). Thus, at higher values of controlling parameters, the height of the channel at the junction decreases due to which smaller droplets are generated. At a fixed flow rate ratio $r = 0.5$, the effect of the controlling parameter and the viscosity ratio λ on the droplet size is depicted in Fig. 7. For a fixed viscosity ratio λ , the droplet size reduces with increase in the controlling parameter. Similarly, at a fixed value of controlling parameter, the droplet size decreases with increase in the viscosity ratio. At a fixed controlling phase flow rate of $1.0 \mu\text{L}/\text{min}$, the value of K_p is different for different flow rate ratios, as shown by the points P_1 to P_3 in Fig. 6b. This is because with the change in flow rate ratios, the effective viscosity of the droplet phase changes and hence there is a change in the pressure jump Δp_i across the thin membrane wall at the junction which leads to different values of K_p . The controlling parameter K_p is a dynamic parameter which changes

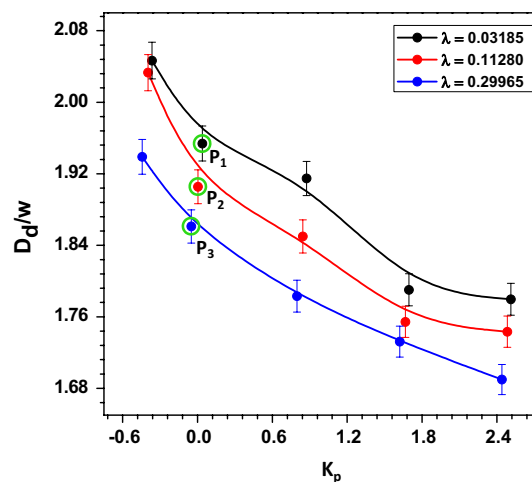


Fig. 7 Non-dimensional droplet size with the controlling parameter at various viscosity ratios for a flow rate ratio of $r = 0.5$, solid line shows fitting of the experimental data; the points circled with the green lines show the points corresponding the controlling phase flow rate $Q_{ctrl} = 1 \mu\text{L}/\text{min}$ (color figure online)

with the change in the flow rate ratio and viscosity ratio of the droplet phase even if the controlling phase flow rate is kept constant.

Using a large set of experimental data, we develop a correlation between non-dimensional droplet size D_d/w , flow rate ratio r , viscosity ratio λ and controlling parameter K_p using Datafit software with a R^2 value of 0.97 and confidence interval of 95 %, which is given as follows

$$\frac{D_d}{w} = k_1(1 + K_p)^{k_2} r^{k_3} \lambda^{k_4} \quad (13)$$

where $k_1 = 1.97064$, $k_2 = -0.0655$, $k_3 = 0.13593$, $k_4 = -0.0273$. As observed, droplet size is a strong

function of flow rate ratio (power coefficient k_3 is the highest). However, the droplet size is a very weak function of the viscosity ratio with a small power coefficient of 0.027. Equation 13 can be used to find out the diameter of the droplet formed in a controlling deformable droplet generator for a set of governing parameters including flow rate ratio, viscosity ratio and flexural rigidity of the membrane. First, from the flow rate ratio of the discrete phase to the continuous phase, the effective viscosity of the sample is determined. Next, the pressure drop across the thin membrane can be determined by using Eqs. 6 and 7. This pressure drop along with the width of the channel and flexural rigidity of the membrane material (Eq. 12) can provide the controlling parameter using Eq. 11. As discussed, when the controlling parameter $K_p = 0$, the membrane deflection is zero and thus the droplet generation behavior of the deformable droplet generator is same as that using a rigid droplet generator. In the above correlation, $K_p = 0$ predicts the droplet size generated using a rigid droplet generator.

5.4 Droplets smaller than junction size

As discussed in the introduction section, the minimum size of droplets formed in a droplet generator is limited by the dimensions of the droplet breakup junction and it is extremely difficult to produce stable droplets of size smaller than the junction size. In the present study, we have used flow-focusing droplet generator to produce droplets of size smaller than the junction size in the dripping regime, which produces stable and homogeneous droplets. The junction size at the droplet breakup junction is controlled by adjusting the membrane deflection at the junction to generate droplets of size smaller than the junction size, as shown in Fig. 8. In our device, the droplet generator junction size is $100 \times 100 \mu\text{m}$. Figure 8a shows the experimental images of the droplets in region A obtained at different values of the controlling parameters. The images attached to the data points in Fig. 8b show the droplet moving through the region B. As explained in Sect. 2, the channel opens up in region B so that the droplets get relaxed into their spherical shape and their sizes could be measured. As observed, the size of the droplets ($135 \pm 6 \mu\text{m}$) using the deformable droplet generator for a controlling parameter value of $K_p = 0$ is same as that obtained using a rigid microchannel ($137 \pm 7 \mu\text{m}$). It is observed that the size of the droplets formed decreases with increase in the controlling parameter. For a controlling parameter $K_p = 1.695$, the size of the droplets generated is $90 \pm 4 \mu\text{m}$, which is smaller as compared to the junction size of $100 \pm 2 \mu\text{m}$. Further, at controlling parameter value of $K_p = 7.79$, droplets of size $75 \pm 3.5 \mu\text{m}$ are generated. The variation of the non-dimensional droplet size D_d/w with the controlling parameter K_p is depicted in Fig. 8b. As observed, the

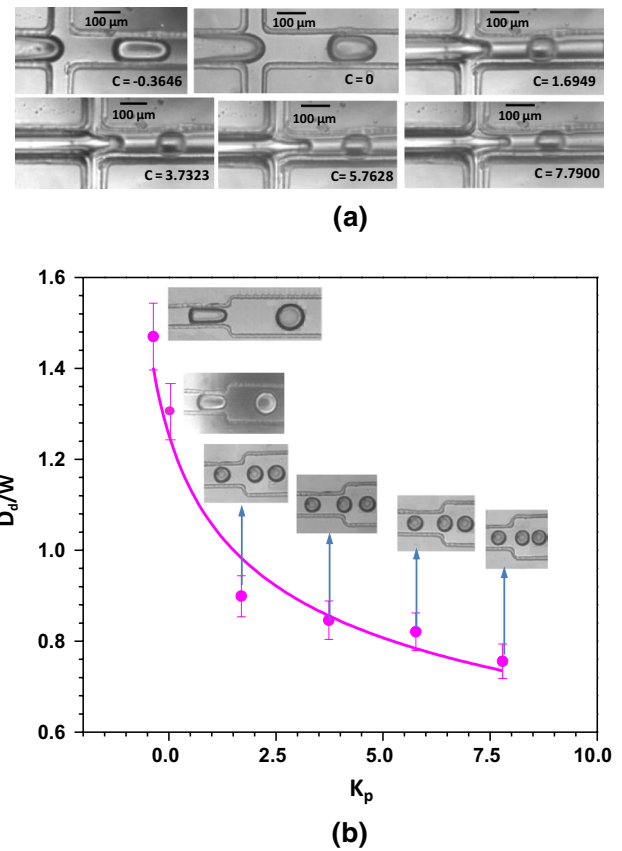


Fig. 8 Generation of droplets of size smaller than junction size. **a** Images of region A at various controlling parameters, sudden change in droplet size is observed from $K_p = 0$ to $K_p = 1.69$. **b** Non-dimensional droplet size variation with the controlling parameter flow rate ratio $r = 0.5$, viscosity ratio $\lambda = 0.03$ and $Ca = 0.027$. Images attached to the data points show the experimental images of droplets produced in the region B; solid line shows fitting of the experimental data

size of the droplets decreases with increase in the value of the controlling parameter K_p . However, beyond a particular value of the controlling parameter K_p , the decrease in the droplet size with increase in K_p becomes negligible. This is because the rate of increase of membrane deflection with increase in the pressure gradient becomes negligible at large deflections, as reported earlier (Raj and Sen 2016).

5.5 Stable and homogeneous droplets at higher Ca

Next, we investigate the droplet generation regimes using the flow-focusing deformable droplet generator. In order to vary the capillary number, we have varied the flow rate of the continuous phase (i.e., mineral oil). As discussed, at low capillary numbers, droplet breakup occurs in the dripping regime, which is stable and hence produces monodisperse droplets in a rigid droplet generator. However, beyond a critical capillary number, the droplet generation occurs in

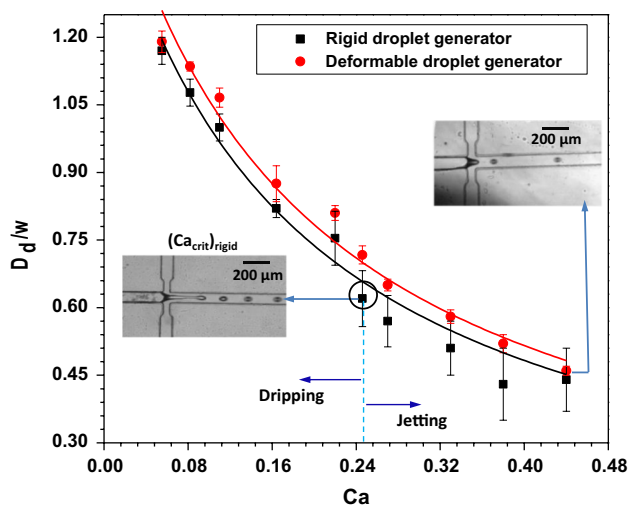


Fig. 9 Non-dimensional droplet size produced at various capillary numbers Ca using a rigid and deformable droplet generator (of same size), the transition from dripping to jetting regime is delayed (i.e., occurs at a higher capillary number in case of a deformable droplet generator), $\lambda = 0.03$, images pictorially show the generation regimes (dripping or jetting), solid line shows fitting of the experimental data

the jetting regime, which is unstable and results in polydisperse droplets. As shown in Fig. 9, in our experiments with a rigid droplet generator microchannel, we observe generation of droplets in the dripping regime up to $Ca = 0.24$ and for $Ca > 0.24$, the droplets are generated in the jetting regime in the case of a rigid droplet generator. At higher $Ca \gg 0.24$, since the droplet breakup phenomena are in the jetting regime, which is quite unstable, it gives rise to large errors in the generated droplet sizes. The large errors in the data shown in Fig. 9 indicate polydispersity of droplets at large Ca in case of rigid droplet generators. However, as shown in Fig. 9, it was possible to generate droplets in the stable dripping regime using a deformable microchannel, even at Ca as high as 0.45. The monodisperse droplets formed using the deformable droplet generator is observed from the small variation in the data points. For example, the size of the droplets produced by using deformable droplet generator at $Ca = 0.45$ was measured to be $43 \pm 2 \mu\text{m}$, which is quite stable and monodisperse.

The droplet generation in the deformable droplet generator is influenced by the controlling parameter. As the capillary number Ca (which is based on the continuous phase flow rate) increases, the effective controlling parameter of the two-phase flow in the droplet channel increases (Fig. 4a), which leads to a different value of pressure drop which modifies the pressure jump across the membrane wall at the junction Δp_r . The deformability of the membrane wall at the junction allows it to expand in case of a change in the pressure inside the droplet phase channel and relieves the stresses generated on the droplet being formed.

When the continuous phase tries to shear off the droplet, unlike in the rigid channel, in the deformable droplet generator, droplet gets a chance to release its stress because of the deformability of the membrane wall. Hence, even at higher capillary number, droplet is able to release the stress and avoid the jetting regime even at higher capillary numbers ($Ca = 0.45$). Also, the wall deformability gives a relief to the droplet when there is pressure fluctuation around the droplet giving rise to the formation of more stable and monodisperse droplet formation. Polydispersity in the droplet size is defined as the ratio of the standard deviation in the size of the droplets to the average size of the droplets. Figure 10 shows a comparison of the polydispersity in the droplet size produced using the rigid versus deformable droplet generators. The results clearly show that the polydispersity of the droplet produced using a deformable droplet generator is much smaller as compared to that using a rigid droplet generator. A reduction of more than 50 % in the polydispersity value can be observed as compared to that of a rigid droplet generator of identical dimensions. In our case, polydispersity value was measured to be 0.015 at $Ca = 0.22$, which compares well with that obtained for a single-layer soft microchannel droplet generator reported by Pang et al. (2014). Figure 10 shows a comparison of the polydispersity in the droplet size produced using the rigid versus deformable droplet generators.

Monodisperse droplets with uniform interdistance between them are required for many applications including chemical industry, pharmaceutical and biology. Frequency of droplet generation can be increased by increasing the Ca number (i.e., increasing the continuous phase flow rate). But, in the case of rigid droplet generators, at high Ca numbers, the droplet breakup occurs in the jetting regime,

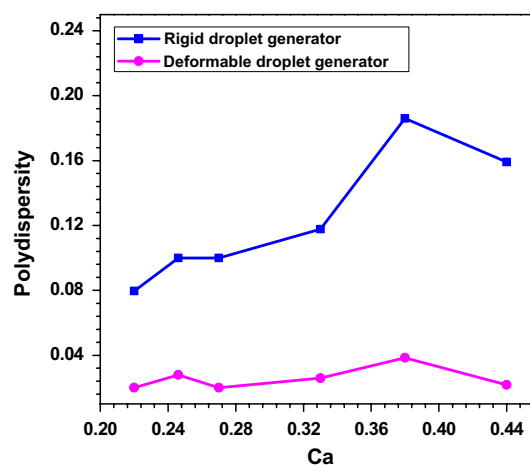


Fig. 10 Comparison of polydispersity of droplets produced using the rigid droplet generator versus the deformable droplet generator at various continuous phase flow rates, solid line shows fitting of the experimental data, all the experiments were conducted at $Q_d = 1 \mu\text{L}/\text{min}$

which increases the droplet polydispersity. In order to ensure monodispersity, lower Ca number needs to be used but it affects the droplet throughput. On the other hand, in case of a deformable microchannel, the jetting regime can be delayed to a higher Ca number and thus the device throughput can be increased while ensuring monodisperse droplet generation. As shown in Fig. 9, as compared to a droplet generator with rigid walls, in the case of a droplet generator with deformable walls, the critical Ca number at which the droplet breakup transit from dripping to jetting regime is higher. This provides the experimental evidence that use of membrane walls provides monodisperse and high-throughput droplet generation.

5.6 Droplet mobility

The droplet mobility study was carried out using a T-junction droplet generator. The droplet mobility ϕ is defined as the ratio of droplet velocity U_d to the superficial velocity of the medium U_T (Sajeesh et al. 2014). The variation of droplet mobility along the flow direction for different values of the controlling parameter K_p is presented in Fig. 11. In a rigid channel, the droplet mobility remains constant along the flow direction but in a deformable channel, due to a gradient in the channel height along the flow direction, the droplet mobility varies. Due to a smaller gradient of the pressure difference across the membrane wall along the flow direction, the variation of membrane deflection is negligible along the microchannel and thus a smaller variation in the droplet mobility. At a fixed location, the effect of the controlling parameter K_p on the droplet mobility can be seen in Fig. 11. It is observed that the mobility first increases, when the controlling parameter increases from

0.021 to 0.036, but when K_p is increased further to 0.050 the droplet mobility decreases. As the controlling parameter increases, the cross-sectional area of the droplet channel reduces, which increases the droplet velocity to keep the mass flow rate constant. This leads to a higher droplet mobility at a higher controlling parameter. An increase in the controlling parameter increases the droplet velocity, but simultaneously it also increases the continuous phase velocity. Thus, at much higher value of the controlling parameter, a decrease in the droplet mobility is observed. The droplet mobility for a rigid channel of identical cross section was measured to be 1.22, which matches with the mobility measured using the deformable microchannel with $K_p = 0$.

6 Conclusion

The droplet generation behavior of a deformable microfluidic droplet generator is presented. The deflection of the external pressure actuated membrane enabled the control of droplet size even smaller than junction size, generation of stable and monodisperse droplets even at higher Ca . The effective height of the channel at different locations along the channel was predicted using the analytical model and compared with experimental data, which showed good agreement within 5 %. The membrane deflection at the junction of the droplet generator for different values of the controlling parameter was measured from experiments and predicted using the analytical model, which showed agreement within 20 %. The effect of controlling parameter K_p on the droplet size was studied for different flow rate ratios and droplet viscosity ratios. It was observed that the droplet diameter decreases with increase in the controlling parameter. At a fixed controlling parameter, the droplet diameter is higher for a higher flow rate ratio and lower viscosity ratio. The droplet diameter was correlated with the controlling parameter, flow rate ratio and the viscosity ratio, which showed stronger dependency with the controlling parameter and weak dependency with the viscosity ratio. The deformable droplet generator was used for generating droplets of sizes lesser (up to 25 %) than that of the junction size, which is difficult to achieve using rigid droplet generators. In case of the deformable droplet generator, due to the deflection of the membrane wall, the transition from the stable dripping regime to the unstable jetting regime is delayed to a higher capillary number Ca , thus pushing the stable high throughput limit. In a rigid channel, above a critical $Ca = 0.24$, the droplet generation shifts from a stable dripping regime to unstable jetting regime which provides higher droplet polydispersity. At the same experimental condition, a deformable droplet generator enables droplet generation in a stable dripping regime, even at

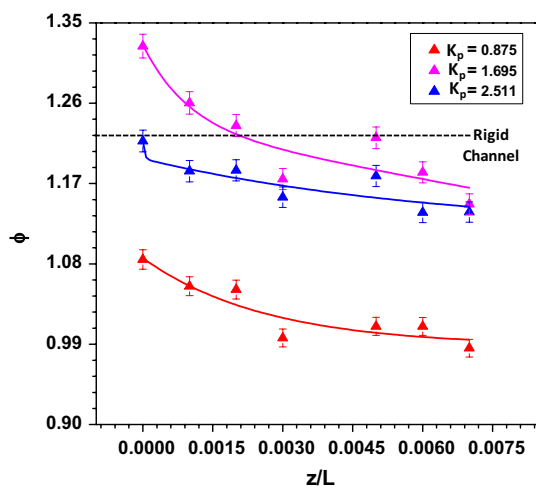


Fig. 11 Mobility of the droplet along the channel length at various controlling parameters, *solid line* shows fitting of the experimental data

$Ca = 0.45$. The polydispersity of the droplets generated using the deformable droplet generators was studied, and it was found that deformable droplet generators provide more than 50 % reduction in the polydispersity of the droplets as compared to the rigid droplet generators. Mobility of the droplets through the deformable microchannel was studied, which showed that droplet mobility initially increases with increase in the controlling parameter (from $K_p = 0.875$ – 1.695) but at much higher controlling parameter ($K_p = 2.511$), the droplet mobility decreases. The deformable droplet generator enabled generation of droplets of size smaller than the junction size by adjusting the controlling parameter. Using a deformable droplet generator of junction size $100 \times 100 \mu\text{m}$, we could obtain droplets of size $45 \mu\text{m}$ in the dripping regime.

Acknowledgments This work was supported by the Indian Institute of Technology Madras via Project No. ERP1314018RESFASHS. The authors also acknowledge the CNRP, IIT Madras for supporting the photolithography work.

Appendix

In order to find an expression for Δh_{max} in terms of the local pressure gradient $p_d(z) - p_c(z)$ across the membrane, we perform force balance on an infinitesimally small strip of the membrane wall of length dz , as shown in Fig. 12b. Depending upon the pressure gradient across the membrane, it will deflect in the direction of lesser pressure. In this case, here we are taking a case where pressure in the droplet channel is higher than in controlling channel, which results in the outward deflection of the membrane increasing the height of the channel. The force acting on the membrane due to the pressure difference across the membrane F_p is balanced by the restoring force F_r that holds the membrane on the bulk PDMS. The lateral component of this restoring force $F_r \cos \alpha$ cancels out due to symmetry (as there is no lateral movement of the membrane). The vertical component of the force due to pressure difference F_p and the restoring force $F_r \sin \alpha$ balance each other as follows,

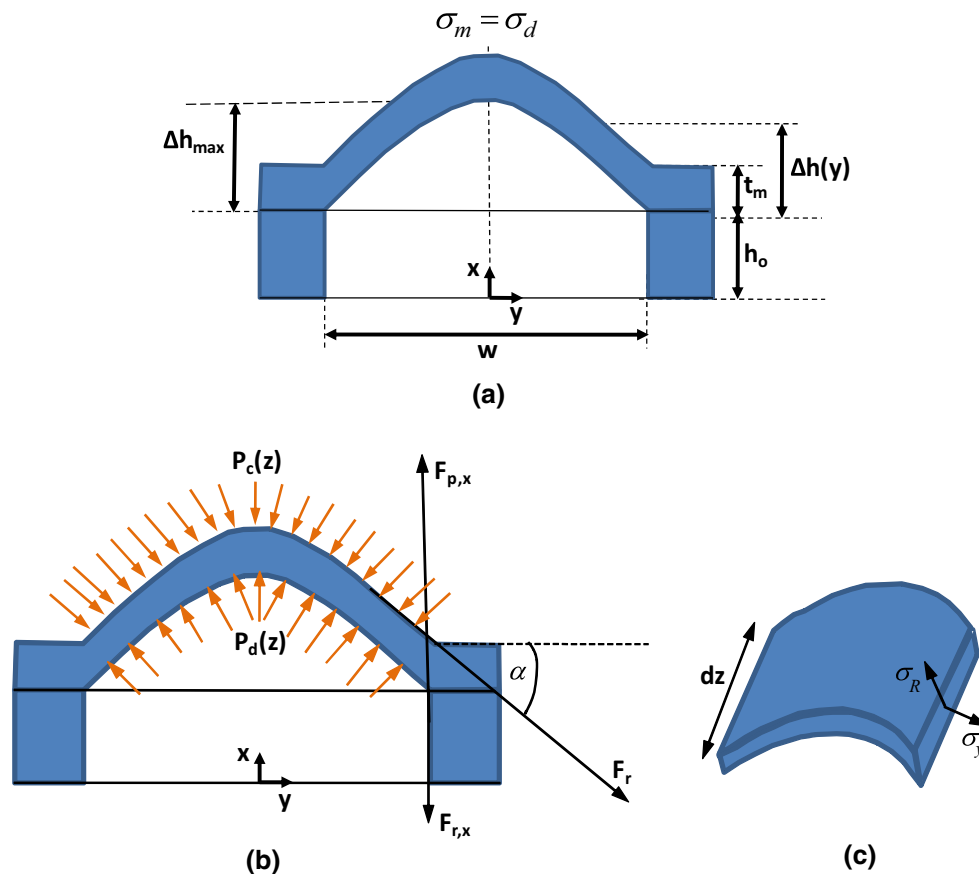


Fig. 12 **a** Parabolic shape of deformed thin wall at a positive discharge condition. **b** Forces and **c** stresses acting on an infinitesimal strip of membrane wall

$$\begin{aligned}
 [p_d(z) - p_c(z)] (w dz) &\approx -\sigma_m (2 dz t_m) \sin \alpha \\
 &= -\sigma_m (2 dz t_m) \left. \frac{\partial(\Delta h)}{\partial y} \right|_{y=w/2} \quad (14)
 \end{aligned}$$

Here, the pressure force F_p is calculated as pressure $p(z)$ times the elemental membrane area $w dz$ and the restoring force F_r is calculated as the membrane stress σ_m time the cross section of the membrane around both the rims $2 dz t_m$ (which is twice the membrane thickness t_m time the elemental length dz). For small angles α , the sine is approximated as the tangent which is the slope of the membrane at its edges and can be found by calculating the derivative of the deflection curve at the rim of the membrane as $\partial(\Delta h)/\partial y|_{y=w/2} = -4(\Delta h_{\max})/w$. Next, by solving for the pressure $p(z)$, we get

$$p_d(z) - p_c(z) = \frac{8\sigma_m t_m \Delta h_{\max}}{w^2} \quad (15)$$

The stress in the membrane wall (Fig. 12c) is a combination of residual stress σ_0 which may be already present when there is no deflection of the membrane and the stress σ_d due to Hooke’s law generated by the deflection of the membrane (Schomburg 2011). Assuming zero residual stress in the membrane, we get

$$\sigma_m = \sigma_d \quad (16)$$

The stresses due to membrane deflection σ_d can be calculated from the strains ε_y and ε_R in the transverse and radial directions, respectively (since, $L \gg w$, the strain in the longitudinal direction is neglected). Now, according to Hooke’s law, the strains ε_y and ε_R can be expressed as

$$\varepsilon_y = \frac{1}{E_m} (\sigma_y + \nu_m \sigma_R) \quad (17)$$

$$\varepsilon_R = \frac{1}{E_m} (\sigma_R + \nu_m \sigma_y) \quad (18)$$

where ν_m and E_m denote Poisson’s ratio and Young’s modulus of the membrane, respectively. For thin membranes, transverse strain is assumed to be constant over the entire membrane (Schomburg 2011) which can be estimated by the extension of the membrane along the neutral fiber of the membrane. The length of the resulting parabola in the deflected state of the membrane is given as (Bronstein and Semendjajew 1976)

$$L_{pa} \approx w \left[1 + \frac{8}{3} \left(\frac{\Delta h_{\max}}{w} \right)^2 - \frac{32}{5} \left(\frac{\Delta h_{\max}}{w} \right)^4 \right] \quad (19)$$

From the above expression of the extended length of the parabola and undeformed width of the membrane w and by

using the assumption $\Delta h_{\max} \ll y_0$, the transverse strain ε_y can be obtained as

$$\varepsilon_y \approx \frac{L_{pa} - w}{w} = \frac{8}{3} \left(\frac{\Delta h_{\max}}{w} \right)^2 \quad (20)$$

The fact that the radial strain is still unknown is resolved using one of the two assumptions (Schomburg 2011) (1) transverse and radial strains are equal throughout the membrane (2) transverse strain is zero throughout the membrane. The second assumption is invalid in the present case as the membrane has a deflection profile along the y -direction thus is subjected to nonzero transverse strain. Assuming that the tangential and radial strain are equal in magnitude throughout the membrane (transverse strain is tensile in nature but radial stress is compressive in nature, which results in $\varepsilon_R = -\varepsilon_y$), from Eqs. 17 and 18, we get,

$$\sigma_y = \varepsilon_y \left(\frac{E_m}{1 - \nu_m} \right) = \sigma_m \quad (21)$$

Finally, using Eqs. 15, 20 and 21, we get

$$p_d(z) - p_c(z) \approx \frac{64}{3} \frac{t_m E_m}{w (1 - \nu_m)} \left(\frac{\Delta h_{\max}}{w} \right)^3 \quad (22)$$

By rearranging the terms in the above equation, we get the expression relating Δh_{\max} with the pressure gradient across the membrane wall at the location, which is as follows.

$$\Delta h_{\max} = \left(\frac{3 w^4 (1 - \nu_m) [p_d(z) - p_c(z)]}{64 t_m E_m} \right)^{\frac{1}{3}}$$

References

Adzima BJ, Velankar SS (2006) Pressure drops for droplet flows in microfluidic channels. *J Micromech Microeng* 16:1504–1510. doi:10.1088/0960-1317/16/8/010

Anoop R, Sen AK (2015) Capillary flow enhancement in rectangular polymer microchannels with a deformable wall. *Phys Rev E Stat Nonlinear Soft Matter Phys* 92:013024. doi:10.1103/PhysRevE.92.013024

Baroud CN, Gallaire F, Danguel R (2010) Dynamics of microfluidic droplets. *Lab on a chip*. doi:10.1039/c001191f

Bronstein IN, Semendjajew KA (1976) *Taschenbuch der Mathematik*. 17 Auflage ISBN 3 87144 0167

Bruus H (2007) *Theoretical microfluidics*. Oxford University Press, New York

Chabert M, Viovy J-L (2008) Microfluidic high-throughput encapsulation and hydrodynamic self-sorting of single cells. *Proc Natl Acad Sci USA* 105:3191–3196

Charcosset C, Limayem I, Fessi H (2004) The membrane emulsification process—a review. *J Chem Technol Biotechnol* 79:209–218. doi:10.1002/jctb.969

Cheung P, Toda-Peters K, Shen AQ (2012) In situ pressure measurement within deformable rectangular polydimethylsiloxane

- microfluidic devices. *Biomicrofluidics* 6:26501–2650112. doi:10.1063/1.4720394
- Christopher GF, Anna SL (2007) Microfluidic methods for generating continuous droplet streams. *J Phys D Appl Phys* 40:R319–R336. doi:10.1088/0022-3727/40/19/R01
- Garstecki P, Stone HA, Whitesides GM (2005) Mechanism for flow-rate controlled breakup in confined geometries: a route to monodisperse emulsions. *Phys Rev Lett* 94:164501. doi:10.1103/PhysRevLett.94.164501
- Garstecki P, Fuerstman MJ, Stone HA, Whitesides GM (2006) Formation of droplets and bubbles in a microfluidic T-junction—scaling and mechanism of break-up. *Lab Chip* 6:437–446. doi:10.1039/b510841a
- Gupta A, Kumar R (2009) Effect of geometry on droplet formation in the squeezing regime in a microfluidic T-junction. *Microfluid Nanofluidics* 8:799–812. doi:10.1007/s10404-009-0513-7
- Gupta A, Kumar R (2010) Flow regime transition at high capillary numbers in a microfluidic T-junction: viscosity contrast and geometry effect. *Phys Fluids* 22:122001. doi:10.1063/1.3523483
- Hsiung S-K, Chen C-T, Lee G-B (2006) Micro-droplet formation utilizing microfluidic flow focusing and controllable moving-wall chopping techniques. *J Micromech Microeng* 16:2403–2410. doi:10.1088/0960-1317/16/11/022
- Huebner A, Sharma S, Srisa-Art M et al (2008) Microdroplets: a sea of applications? *Lab Chip* 8:1244–1254. doi:10.1039/b806405a
- Johnston ID, McCluskey DK, Tan CKL, Tracey MC (2014) Mechanical characterization of bulk Sylgard 184 for microfluidics and microengineering. *J Micromech Microeng* 24:035017. doi:10.1088/0960-1317/24/3/035017
- Kemna EWM, Schoeman RM, Wolbers F (2012) High-yield cell ordering and deterministic cell-in-droplet encapsulation using Dean flow in a curved microchannel. *Lab Chip* 12:2881–2887. doi:10.1039/c2lc00013j
- Kohler JM, Henkel T (2005) Chip devices for miniaturized biotechnology. *Appl Microbiol Biotechnol* 69:113–125
- Landau LD, Lifshitz EM (1986) *Theory of elasticity*. Pergamon Press, Oxford
- Lee C-H, Hsiung S-K, Lee G-B (2007) A tunable microflow focusing device utilizing controllable moving walls and its applications for formation of micro-droplets in liquids. *J Micromech Microeng* 17:1121–1129. doi:10.1088/0960-1317/17/6/004
- Lignel S, Drelich A, Sunagatullina D et al (2014) Differential scanning calorimetry analysis of W/O emulsions prepared by miniature scale magnetic agitation and microfluidics. *Can J Chem Eng* 92:337–343. doi:10.1002/cjce.21925
- Lin Y-H, Lee C-H, Lee G-B (2008) Droplet formation utilizing controllable moving-wall structures for double-emulsion applications. *J Microelectromech Syst* 17:573–581. doi:10.1109/JMEMS.2008.924273
- Link DR, Grasland-Mongrain E, Duri A (2006) Electric control of droplets in microfluidic devices. *Angew Chem Int Ed Engl* 45:2556–2560. doi:10.1002/anie.200503540
- Liu M, Sun J, Sun Y (2009) Thickness-dependent mechanical properties of polydimethylsiloxane membranes. *J Micromech Microeng* 19:035028. doi:10.1088/0960-1317/19/3/035028
- Meesters G, Vercoulen P, Marijnissen J, Scarlett B (1992) Generation of microj-sized droplets from the Tylor cone. *J Aerosol Sci* 23:37–49
- Nie Z, Seo M, Xu S (2008) Emulsification in a microfluidic flow-focusing device: effect of the viscosities of the liquids. *Microfluid Nanofluidics* 5:585–594. doi:10.1007/s10404-008-0271-y
- Pang Y, Kim H, Liu Z, Stone HA (2014) A soft microchannel decreases polydispersity of droplet generation. *Lab Chip* 14:4029–4034. doi:10.1039/c4lc00871e
- Raj A, Sen AK (2016) Flow-induced deformation of deformable microchannels and its effect on pressure–flow characteristics. *Microfluid Nanofluidics* 20:31. doi:10.1007/s10404-016-1702-9
- Reznik N, Williams R, Burns PN (2011) Investigation of vaporized submicron perfluorocarbon droplets as an ultrasound contrast agent. *Ultrasound Med Biol* 37:1271–1279. doi:10.1016/j.ultrasmedbio.2011.05.001
- Sajeesh P, Doble M, Sen AK (2014) Hydrodynamic resistance and mobility of deformable objects in microfluidic channels. *Biomicrofluidics* 8:1–23. doi:10.1063/1.4897332
- Sarrazin F, Prat L, Di Miceli N, Cristobal G, Link DR (2007) Mixing characterization inside microdroplets engineered on a microcoalescer. *Chem Eng Sci* 62:1042–1048
- Schomburg WK (2011) *Introduction to microsystem design*. Springer. ISBN 978-3-642-19488-7
- Sen AK, Darabi J (2007) Droplet ejection performance of a monolithic thermal inkjet print head. *J Micromech Microeng* 17:1420
- Sugiura S, Nakajima M, Iwamoto S, Seki M (2001) Interfacial tension driven monodispersed droplet formation from microfabricated channel array. *Langmuir* 17:5562–5566. doi:10.1021/la010342y
- Surya HPN, Parayil S, Banerjee U et al (2014) Alternating and merged droplets in a double T-junction microchannel. *BioChip J*. doi:10.1007/s13206-014-9103-1
- Thangawng AL, Ruoff RS, Swartz MA, Glucksberg MR (2007) An ultra-thin PDMS membrane as a bio/micro–nano interface: fabrication and characterization. *Biomed Microdevices* 9:587–595. doi:10.1007/s10544-007-9070-6
- Umbanhowar PB, Prasad V, Weitz DA (2000) Monodisperse emulsion generation via drop break off in a coflowing stream. *Langmuir* 16:347–351. doi:10.1021/la990101e
- Van der Graaf S, Nisisako T, Schroën CGPH (2006) Lattice Boltzmann simulations of droplet formation in a T-shaped microchannel. *Langmuir* 22:4144–4152. doi:10.1021/la052682f
- Vehring R, Foss WR, Lechuga-Ballesteros D (2007) Particle formation in spray drying. *J Aerosol Sci* 38:728–746. doi:10.1016/j.jaerosci.2007.04.005
- Vladisavljevic GT, Khalid N, Neves MA (2013) Industrial lab-on-a-chip: design, applications and scale-up for drug discovery and delivery. *Adv Drug Deliv Rev* 65:1626–1663. doi:10.1016/j.addr.2013.07.017
- Yang CG, Xu ZR, Wang JH (2010) Manipulation of droplets in microfluidic systems. *TrAC Trends Anal Chem* 29:141–157. doi:10.1016/j.trac.2009.11.002
- Yoshida J, Ohmori K, Takeuchi H (2005) Treatment of ischemic limbs based on local recruitment of vascular endothelial growth factor-producing inflammatory cells with ultrasonic microbubble destruction. *J Am Coll Cardiol* 46:899–905
- Zhang DF, Stone HA (1997) Drop formation in viscous flows at a vertical capillary tube. *Phys Fluids* 9:2234. doi:10.1063/1.869346